Eur Biophys J (2011) 40:627–639
DOI 10.1007/s00249-010-0663-2

ORIGINAL PAPER

Quantitative prediction of the arrhythmogenic effects of de novo hERG mutations in computational models of human ventricular tissues

Alan P. Benson · Moza Al-Owais · Arun V. Holden

Received: 11 October 2010 / Revised: 13 December 2010 / Accepted: 20 December 2010 / Published online: 14 January 2011

Abstract Mutations to hERG which result in changes to the rapid delayed rectifier current I_{Kr} can cause long and short QT syndromes and are associated with an increased risk of cardiac arrhythmias. Experimental recordings of I_{Kr} reveal the effects of mutations at the channel level, but how these changes translate to the cell and tissue levels remains unclear. We used computational models of human ventricular myocytes and tissues to predict and quantify the effects that de novo hERG mutations would have on cell and tissue electrophysiology. Mutations that decreased I_{Kr} maximum conductance resulted in an increased cell and tissue action potential duration (APD) and a long QT interval on the electrocardiogram (ECG), whereas those that caused a positive shift in the inactivation curve resulted in a decreased APD and a short QT. Tissue vulnerability to re-entrant arrhythmias was correlated with transmural dispersion of repolarisation, and any change to this vulnerability could be inferred from the ECG QT interval or T wave peak-to-end time. Faster I_{Kr} activation kinetics caused cell APD alternans to appear over a wider range of pacing rates and with a larger magnitude, and spatial heterogeneity in these cellular alternans resulted in discordant alternans at the tissue level. Thus, from channel kinetic data, we can predict the tissue-level electrophysiological effects of any hERG mutations and identify how the mutation would manifest clinically, as either a long or short QT syndrome with or without an increased risk of alternans and re-entrant arrhythmias.

Keywords Cardiac arrhythmia · Computational modelling · Human ether-a-go-go-related gene · hERG · Long QT syndrome · Short QT syndrome

Abbreviations

APD	Action potential duration
cNBD	Cyclic nucleotide binding domain
ECG	Electrocardiogram
hERG	Human ether-a-go-go-related gene
I_{Kr}	Rapid delayed rectifier potassium current
LQTS	Long QT syndrome
M	Midmyocardial
PAS	Per-Arnt-Sim
SQTS	Short QT syndrome
TDR	Transmural dispersion of repolarisation
VF	Ventricular fibrillation
WT	Wild type

A. P. Benson and M. Al-Owais have contributed equally to this work.

A. P. Benson (✉) · A. V. Holden
Institute of Membrane & Systems Biology,
and Multidisciplinary Cardiovascular Research Centre,
University of Leeds, Leeds LS2 9JT, UK
e-mail: a.p.benson@leeds.ac.uk

M. Al-Owais
Division of Cardiovascular & Neuronal Remodelling,
and Multidisciplinary Cardiovascular Research Centre,
University of Leeds, Leeds LS2 9JT, UK

Introduction

The inherited long (LQTS) and short (SQTS) QT syndromes are associated with an increased probability of re-entrant cardiac tachyarrhythmias such as ventricular fibrillation (VF) that, in some cases, may cause sudden death (Morita et al. 2000). The altered QT interval of the electrocardiogram (ECG) is due to early or delayed

repolarisation of the ventricular action potential. Mutations in the human ether-a-go-go-related gene (hERG), which encodes the $K_v11.1$ potassium channel, have been implicated in LQTS type 2 (Sanguinetti et al. 1995; Tseng 2001) and SQTS type 1 (Brugada et al. 2004). $K_v11.1$ plays a crucial role in repolarisation of cardiac myocytes, where it results in the rapid delayed rectifier potassium current (I_{Kr}) component of the cardiac action potential (Finlayson et al. 2004). Lengthening of the ventricular action potential can be produced by partial or complete loss of function mutations of hERG (Lehmann-Horn and Jurkat-Rott 1999), and shortening by gain-of-function mutations (Antzelevitch et al. 2007a). However, the effect of these mutations on the underlying potassium channel kinetics remains unclear. In addition, LQTS can be caused by hERG trafficking abnormalities and a resultant down-regulation of I_{Kr} (Thomas et al. 2003), and some drug-induced forms of LQTS, caused by the interactions with $K_v11.1$ of drugs used to treat non-cardiac conditions, have been identified leading to restrictions on the use of certain compounds (e.g. thioridazine and dofetilide) (Recanatini et al. 2008).

The $K_v11.1$ channels are characterised by the long intracellular carboxy- and amino-terminal regions (C and N terminals respectively) of their subunits that modulate gating and affect activation and inactivation. These regions include the cyclic nucleotide binding domain (cNBD) in the C terminal region and a Per-Arnt-Sim (PAS) domain in the N terminal. The cNBD itself hangs as a tetramer below the membrane and is surrounded by other intracellular regions such as the PAS domain, such that the surface regions of the cNBD may interact with other intracellular regions of the channel protein. A homology model of the hERG cNBD tetramer is shown in Fig. 1. Patch clamp studies have helped elucidate the effects on channel function of mutations in the PAS and the cNBD domains of $K_v11.1$ (Akhavan et al. 2005; Al-Owais et al. 2009; Cui et al. 2001; Satler et al. 1996), defining structural and functional interactions of intracellular components of the channel.

Previous experimental (Chen et al. 1999) and computational (Benson et al. 2009; Peitersen et al. 2008) studies have shown that, although the net effect of some mutations in hERG is to produce a lengthening of the action potential, this can be decomposed into effects on the voltage dependence of the channel that serve to shorten as well as prolong the action potential duration (APD). Differences in experimentally recorded I_{Kr} kinetics due to specific mutations of hERG may lead to changes in the emergent whole cell APD and tissue vulnerability to re-entrant arrhythmias. These cell and tissue electrophysiological properties result from non-linear interactions between the many different membrane ionic current systems, and so computational models of cardiac cells and tissues are necessary for quantitative prediction of these arrhythmogenic effects. Computational modelling also allows dissection of the dynamic mechanisms underlying electrophysiological changes produced by hERG mutations, as the differences in I_{Kr} current parameters can be introduced in isolation or in any combination, and their effects at the cell and tissue levels computed.

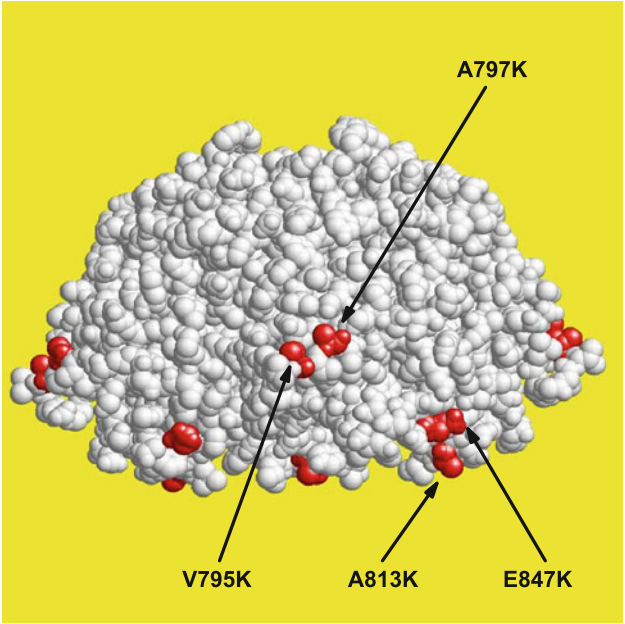

Fig. 1 Homology model of the hERG cNBD tetramer. Residues *highlighted in red* are those that cause significant electrophysiological changes compared with WT. The locations of the four de novo mutations used for the simulations presented here are indicated with *arrows*

Here we extend work presented earlier (Al-Owais et al. 2009), which determined the channel-level electrophysiological effects of a set of de novo mutations in the cNBD. We examined what effects these de novo mutations would have beyond the channel level (i.e. at the cell and tissue levels) by using computational models of human ventricular myocytes and tissues to quantitatively predict the cell action potential and tissue electrophysiology. In particular, we examine how specific mutations affect substrates for re-entrant arrhythmias (electrical alternans and tissue vulnerability) and examine whether changes to tissue vulnerability could be inferred from ECG measures. As there are no clinical data for the de novo mutations that would allow direct validation of our results, we also include in the analysis an R56Q mutation (from the same set of experiments as the de novo mutations) which has previously been identified with LQTS type 2 (Chen et al. 1999). The R56Q mutation therefore acted as a "control mutation" as it should produce a long QT interval in our models, thereby providing validation for the methodology and interpretation we have used with the de novo mutations.

Methods

Electrophysiology

Electrophysiological methods were described in detail previously (Al-Owais et al. 2009). Briefly, mutations were expressed in *Xenopus* oocytes where lysine mutations had been induced in residues in the cNBD and PAS domains (Fig. 1) of wild type (WT) hERG by site-directed mutagenesis. I_{Kr} currents from WT and mutant oocytes bathed in Ringer's solution were then recorded using standard two-microelectrode voltage clamp techniques at room temperature (see Fig. 2 for examples). Peak current (I_{max}) and the voltage dependence of activation were determined from tail currents measured at −40 mV following 1 s depolarisations to test potentials (Fig. 2a). The peak tail currents were fitted with a Boltzmann function in order to determine the half activation voltages ($V_{0.5,act}$) and slopes (k_{act}) of the activation curves. Activation time constants (τ_{act}) were measured using a 1 s pre-pulse to +40 mV followed by a step to a test potential (Fig. 2b); the time course was fit with a double exponential function. The voltage dependence of inactivation was determined using a three-pulse voltage protocol (Numaguchi et al. 2000), with a pre-pulse to +60 mV applied for 3 s to fully inactivate the channels, followed by a 20 ms step to a test potential, with the current measured during a final step to +30 mV (Fig. 2c). A Boltzmann function was fitted to the peak currents in order to determine the half inactivation voltages ($V_{0.5,inact}$) and slopes (k_{inact}) of the inactivation curves.

Computational modelling: isolated cells

For an isopotential cell, the rate of change of membrane potential V (mV) is given by

$$\frac{dV}{dt} = -I_{ion}, \tag{1}$$

where t (ms) is time and I_{ion} (pA pF^{-1}) is the sum of the transmembrane current densities, which in this study was given by the human ventricular cell models of Ten Tusscher and Panfilov (Ten Tusscher and Panfilov 2006). The differing action potentials found in the endocardial, midmyocardial (M) or epicardial regions of the ventricles are modelled by different parameter sets in the equations for I_{ion}. The I_{Kr} component of I_{ion} can be modelled using Hodgkin-Huxley formalism:

$$I_{Kr} = G_{Kr} n_{act} n_{inact} (V - E_K), \tag{2}$$

where G_{Kr} (nS pF^{-1}) is the maximum channel conductance, n_{act} and n_{inact} are activation and inactivation gating variables respectively, and E_K (mV) is the reversal potential for potassium given by the Nernst equation. The dynamic gating variables n_{act} and n_{inact} are given by the differential equation

$$\frac{dn_i}{dt} = \frac{n_{i\infty} - n_i}{\tau_i}, \tag{3}$$

where $n_{i\infty}$ is the steady-state value of the gating variable and τ_i (ms) is an associated time constant, both of which are functions of V. The functions $n_{act\infty}$ and $n_{inact\infty}$

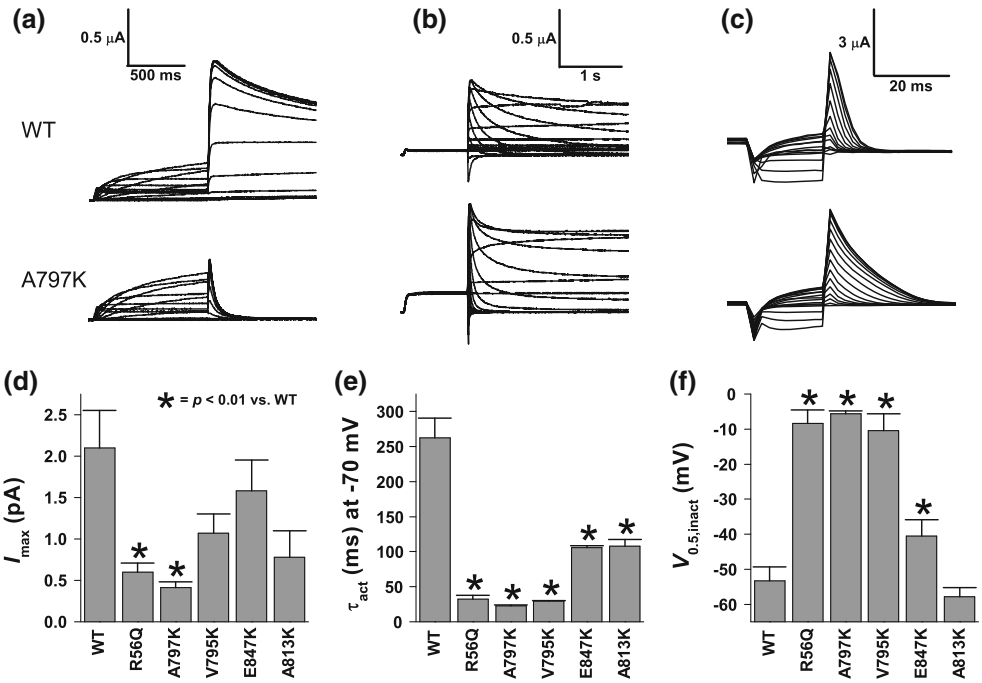

Fig. 2 **a–c** Example I_{Kr} current traces used to calculate peak current, the activation time constant at −70 mV, and the half inactivation voltage respectively in WT and mutant cells. See text for voltage clamp protocols. **d–f** Summary of the experimental data

correspond to the experimentally determined activation and inactivation curves respectively and are described by Boltzmann functions (i.e. by a half activation voltage $V_{0.5}$ and a slope k). Here, as in the Ten Tusscher and Panfilov model for I_{Kr} (Ten Tusscher and Panfilov 2006), the activation time constant τ_{act} corresponds to the fast time constant ($\sim$200 ms at $-$70 mV) of the double exponential fit to experimental activation/deactivation traces. The inactivation time constant τ_{inact}, which has a value of $\sim$1 ms at $-$70 mV, describes the extremely fast channel inactivation kinetics that are responsible for inward rectification.

From voltage clamp recordings of WT and mutated I_{Kr} channels, the peak current I_{max} (which relates to channel conductance G_{Kr}), the half activation voltages $V_{0.5}$ and slopes k of the activation and inactivation curves, and the activation and inactivation time constants τ were determined. Any changes from WT were incorporated into the parameter sets of the cell models, then these models were used to predict, in silico, the effects of the hERG mutations at the cellular level. All cell models were paced 50 times using a 1 ms conservative current stimulus (Hund et al. 2001) with a magnitude twice the diastolic threshold. Equation 1 was solved with a forward Euler method (Press et al. 2009) using an adaptive time step as described by Benson et al. (2008), while equations for gating variables in the form of Eq. 3 were solved with the scheme of Rush and Larsen (1978). APD was measured at 90% repolarisation. APD restitution was measured using a standard S1–S2 protocol, with 50 S1 pacing beats at a cycle length of 1,000 ms and a final S2 beat applied after a variable interval.

Computational modelling: tissues

To predict the tissue-level effects of the mutations, the single-cell models described above were incorporated into a heterogeneous 15 mm one-dimensional transmural strand model of the human left ventricular wall (Benson et al. 2007). For such a one-dimensional virtual tissue, membrane potential is given by

$$\frac{\partial V}{\partial t} = D\frac{\partial^2 V}{\partial x^2} - I_{ion}, \tag{4}$$

where x (mm) is transmural distance along the strand, D (mm^2 ms^{-1}) is a diffusion coefficient that characterises electrotonic spread of membrane potential along the strand, and I_{ion} is given by one of the cell models described above. Each tissue model included regions of endocardial, M and epicardial tissue (that is, I_{ion} was spatially heterogeneous) with widths in the ratio 3:5:7, which gave an upright pseudo-ECG T wave (see "Electrocardiogram") under WT conditions. This spatial distribution is backed by experiments which show that, in the human ventricles, the longest APDs (i.e. those from M cells) are in the deep subendocardium (Glukov et al. 2010). Equation 4 was solved with a forward time centred space method (Press et al. 2009) using an operator splitting and adaptive time step technique (Qu and Garfinkel 1999), with a space step of $\Delta x = 0.2$ mm, a minimum time step of $\Delta t_{min} = 0.01$ ms and a maximum time step of $\Delta T = 0.25$ ms. A value of $D = 0.065$ mm^2 ms^{-1} was selected to give a steady state conduction velocity along the strand (i.e. a transmural conduction velocity) of 0.45 m s^{-1} and a transmural activation time of 30 ms at a pacing cycle length of 1 s, corresponding to values found experimentally in whole human hearts (Durrer et al. 1970) and human ventricular wedge preparations (Glukov et al. 2010).

Electrocardiogram

The ECG was represented by the ventricular electrogram (the pseudo-ECG), computed using

$$\Phi = \frac{a^2}{4}\int(-\nabla V)\left(\nabla\frac{1}{x-x'}\right)\mathrm{d}x, \tag{5}$$

where Φ represents the unipolar potential recorded at an electrode 20 mm from the epicardial end of the strand, $a = 11$ μm is the radius of the fibre, $\nabla \equiv \partial/\partial x$ is a spatial gradient operator, and $x - x'$ is the distance from the electrode to any point in the tissue (Plonsey and Barr 1988). We examined three potential ECG markers of pro-arrhythmia: the QT interval (Lawrence et al. 2005), T wave width (Arini et al. 2008), and the time from the peak to the end of the T wave (T_{peak}–T_{end}) (Antzelevitch et al. 2007b). Because the computed pseudo-ECG traces were smooth, the onset of the QRS complex and the location of the T wave could be detected manually. The morphology of the T wave and its onset, peak and end times were identified from the time derivative of the pseudo-ECG trace using the thresholds described by Martínez et al. (2004). In the case of complex (e.g. biphasic) T waves, the peak time corresponded to the peak or nadir with the largest absolute baseline-corrected value.

Substrates for arrhythmias

We examined the effects of the hERG mutations on two substrates for re-entrant arrhythmias (Lawrence et al. 2005): electrical alternans, a measure of temporal heterogeneities of APD; and the vulnerable window, an index of spatial electrophysiological heterogeneities in a tissue.

Alternans are beat-to-beat variations in APD, where a short action potential is followed by a long action potential, which is then followed by a short action potential, and so on (see Fig. 8a below for an example). APD alternans

manifest as T wave alternans at the ECG level and have been linked to the emergence of VF (Pastore et al. 1999; Weiss et al. 2006). As such, examination of APD alternans at fast pacing rates has been proposed as a method of identifying pro-arrhythmic I_{Kr} alterations (Fossa et al. 2004). We used a dynamic restitution protocol in single-cell and tissue models to identify the pacing rates at which alternans appeared under WT and mutant conditions and the amplitude of these alternans: cells and tissues were paced 50 times starting at a cycle length of 1,000 ms, the last action potentials were examined for any alternans, then cycle length was reduced by 5 ms. Simulations continued until loss of a 1:1 or 2:2 response. In tissues, we also examined whether any alternans were concordant (spatially regular for any given beat) or discordant (spatially irregular for any given beat, with some parts of the tissue exhibiting a short APD while other parts exhibit a long APD): the emergence of discordant alternans is of particular interest, as this has been linked to the initiation of VF due to the development of steep spatial gradients in repolarisation (Pastore et al. 1999; Qu et al. 2000) and a resultant increase in tissue vulnerability (see below).

Ectopic beats (i.e. those that are initiated at abnormal locations and times) are often found in asymptomatic normal subjects, even at rest, but they are relatively benign and usually only lead to premature ventricular contractions. However, occasionally an ectopic excitation can trigger a re-entrant arrhythmia if it occurs within a vulnerable time window. Examples of tissue behaviour in response to ectopic stimuli are shown in Fig. 3. If an ectopic excitation (e.g. an early or delayed afterdepolarisation or triggered activity, but here simulated by applying an ectopic stimulus) occurs early in the normal repolarisation sequence, the ectopic excitation cannot propagate (Fig. 3a). If the ectopic excitation occurs relatively late, bidirectional propagation occurs and so the ectopic excitation propagates to both ends of the strand, which would result in a premature ventricular contraction (Fig. 3b). However, there is a spatio-temporal region where unidirectional block of a propagating action potential can occur, as illustrated in Fig. 3c, which could initiate a pair of re-entrant waves in a two- or three-dimensional tissue [unidirectional block is a necessary condition for the initiation of re-entrant arrhythmias (Jalife 2000)]. This spatio-temporal region of unidirectional block is the vulnerable window (Starmer et al. 1993). An increase in the temporal or spatial width of the vulnerable window will increase the probability that any ectopic excitation that occurs can initiate re-entry, and so measurement of the vulnerable window is one index of the arrhythmogenicity of the tissue. We measured the vulnerable window in each tissue by mapping out the spatio-temporal region where, following 50 endocardial pacing stimuli at a cycle length of 1,000 ms, a second stimulus (with a 1 ms duration, a magnitude four times the diastolic

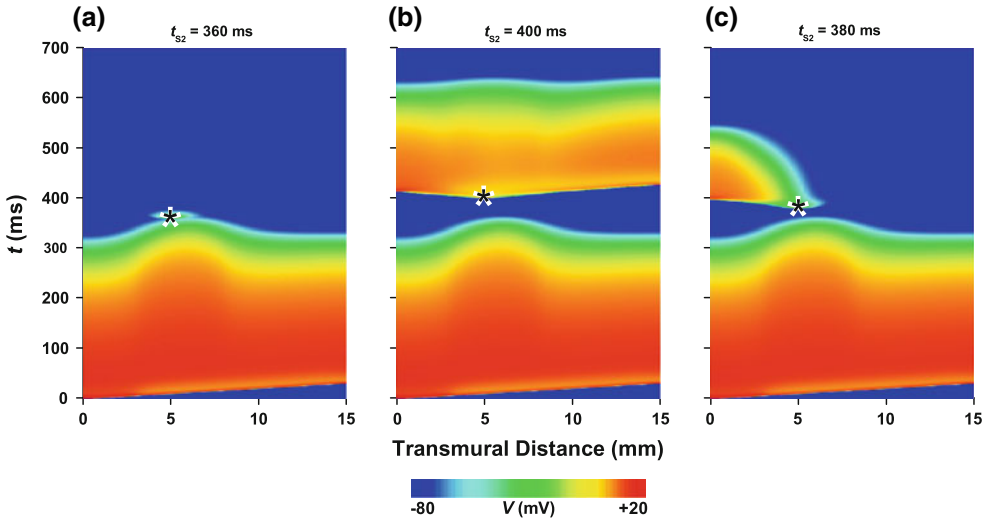

Fig. 3 **a–c** Space-time plots showing tissue behaviour in response to an ectopic excitation. The tissue is first paced from the endocardial end of the strand ($x = 0$ mm) at time $t = 0$ ms. The APD varies throughout the ventricular wall due to the endocardial, midmyocardial (M) and epicardial cell types having different APDs; the M cells here are located between 3 and 8 mm to be consistent with APD distribution in the non-failing human ventricle (Glukov et al. 2010). The ectopic (S2) excitation is applied at some location in the tissue (x_{S2}) at some time during late repolarisation (t_{S2}). Depending on the location and timing of the ectopic stimulus, three behaviours are observed (in the following examples, $x_{S2} = 5$ mm and the spatio-temporal location of the ectopic stimulus is shown by an *asterisk*): **a** propagation of excitation is blocked by refractory tissue, when $t_{S2} = 360$ ms in this example; **b** bidirectional propagation occurs when the ectopic stimulus is applied after the vulnerable window, when tissue either side of the ectopic stimulus site is no longer refractory, in this case $t_{S2} = 400$ ms; **c** unidirectional propagation occurs if the ectopic stimulus is applied in the vulnerable window, here when $t_{S2} = 380$ ms

threshold and applied at different locations within the wall over 0.8 mm of tissue) produced unidirectional propagation.

Statistical analysis

Data were analysed using Origin (OriginLab, Northampton, MA). Experimental patch clamp results are presented as mean ± SE. Significant differences between means of WT and mutant groups were tested for using Student's t tests, while relationships between groups were examined using Pearson correlation coefficients. Values of $P < 0.01$ were considered statistically significant.

Results

Experimental data

Figure 2 shows experimental data obtained from *Xenopus* oocytes injected with WT and mutant hERG RNA. Panels d–f summarise these experimental data for WT, an R56Q mutant and four de novo mutations (A797K, V795K, E847K and A813K). The R56Q mutation replicates a mutation identified with LQTS type 2 (Chen et al. 1999), and thus acting as a "control mutation" as it should produce a long QT interval in our models. The four de novo mutations chosen for the simulations presented here represent a cross-section of the different qualitative behaviours observed with all 22 mutations previously examined experimentally by our group (Al-Owais et al. 2009). The R56Q and A797K mutations both have a decreased peak current, a positively shifted half inactivation voltage and faster activation kinetics compared to WT. The V795K and E847K mutations show positively shifted half inactivation voltages and faster activation kinetics compared to WT but no change in channel conductance. The A813K mutation differs from WT only in that it has faster kinetics. There were no significant differences between any of the half activation voltages, or between the slopes of the activation or inactivation curves (see Al-Owais et al. 2009 for details). Table 1 quantifies these changes and shows the alterations made to the parameter values of mutant cells and tissues in our computational models. Berecki et al. (2005) showed that the magnitude of experimental inactivation curve shifts is temperature-dependent: shifts observed at room temperature are greater than those observed at body temperature. As such, and because our experimental measurements were made at room temperature (21–24°C), we scaled our inactivation curve shifts by 0.45 (cf. Table 1 in Berecki et al. 2005) to give an approximate shift that would have occurred at body temperature. Note that the activation time constant is voltage-dependent and that the mutant time constant formulations are simply scaled from WT values.

Table 1 Model I_{Kr} parameter changes for the R56Q "control mutation" and the four de novo mutations

	G_{Kr} (% of WT)	τ_{act} (% of WT)	$V_{0.5,inact}$ (mV shift)
R56Q	28.4	12.4	+20.2
A797K	19.5	8.6	+21.4
V795K	–	11.2	+19.3
E847K	–	40.3	+5.7
A813K	–	41.0	–

Parameters were altered according to the experimental data shown in Fig. 1. The default published parameter values for the model (Ten Tusscher and Panfilov 2006) were taken as the WT parameters for this study. A *dash* indicates the parameter value is the same as WT

Cell electrophysiology

Figure 4 shows simulated M cell I_{Kr} and corresponding action potentials for WT and mutant virtual cells paced at a cycle length of 1 s, along with APD restitution curves obtained using an S1–S2 protocol. Note that in all panels the A813K traces are overlaid and so effectively indistinguishable from the WT traces. Although we only show data for M cells, we found qualitatively similar results for endocardial and epicardial cells but, for the sake of brevity, do not show these data. Note that the initial spike in each current trace (Fig. 4a), which is present in all cell/mutation types, is also seen experimentally and is due to the inactivation gate responsible for inward rectification being a time-dependent process rather than instantaneous (Ten Tusscher et al. 2004). This initial spike has a larger amplitude with all mutations compared to WT but is particularly large with the V795K de novo mutation due to the relatively fast activation kinetics and relatively large positive shift of the inactivation curve (combined with the normal channel conductance) seen with this mutation. I_{Kr} during the repolarisation phase is reduced in the R56Q and the de novo A795K mutations compared to WT, stays roughly the same with the A813K mutation, and is increased with both the V795K and E847K mutations, with these changes reflected in the cell APDs. As expected from previous experimental (Chen et al. 1999) and computational (Berecki et al. 2005) studies, the R56Q mutation in the model resulted in an increased APD compared to WT (Fig. 4b), from 414 to 450 ms for M cells, an increase of 7%. Only one of the de novo mutations, A797K, resulted in a prolongation of APD. This de novo mutation—like R56Q in that it results in decreased maximum channel conductance, faster activation kinetics and a positive shift in the inactivation curve—caused an 11% APD increase compared to WT in the M cell, taking APD to 469 ms. Two of

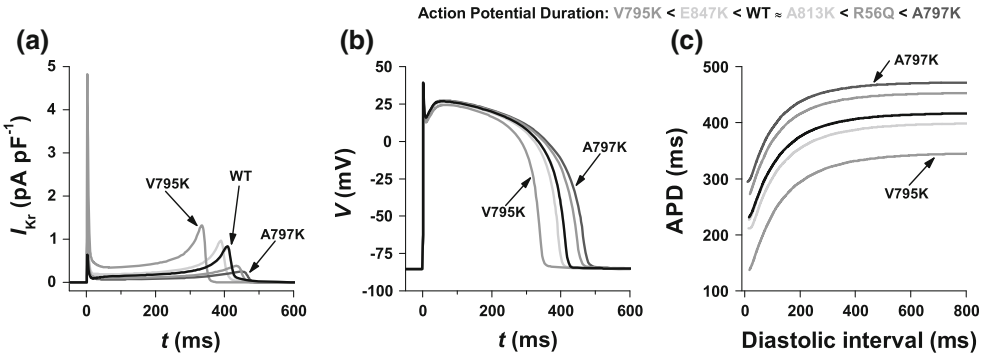

Fig. 4 Simulated periodic state I_{Kr} (**a**) and action potentials (**b**) for WT and mutant midmyocardial (M) cells paced at a cycle length of 1,000 ms. **c** APD restitution curves obtained with an S1–S2 protocol for WT and mutant M cells

the de novo mutations resulted in decreased APD, with V795K producing the largest reduction (to 343 ms, a 17% reduction compared to WT) followed by E847K (a 4% reduction to 396 ms). Both of these mutations result in faster activation kinetics and a shifted inactivation curve but, unlike the mutations causing prolonged APD, do not result in decreased maximum channel conductance. Note also that the V795K mutation, which causes the largest of the two APD reductions, has faster activation kinetics and a greater inactivation curve shift than the E847K mutation. The remaining de novo mutation, A813K, caused effectively no change in APD (a 0.6 ms increase). Unlike the other mutations, A813K only affects the time constant of activation and does not result in a reduced maximum channel conductance or a shift in the inactivation curve. These APD relationships between WT and mutant cells also hold over a large range of pacing cycle lengths, as shown in the APD restitution curves of Fig. 4c.

Pseudo electrocardiograms

As the QT interval of the ECG is determined by the tissue APD, whether a particular mutation will cause a long or a short QT interval will follow from the cell APD restitution curves in Fig. 4. Indeed, we do find this to be the case, with mutations that give the largest APD increases/decreases also resulting in the largest QT interval increases/decreases (compare Figs. 4 and 5). Figure 5a shows the pseudo ECG calculated for WT virtual tissue (which has a QT interval of 369 ms), along with pseudo ECGs from A797K and V795K tissues, which give the longest (405 ms) and shortest (321 ms) QT intervals respectively. Figure 5b shows the T waves calculated for tissues with mutations that cause SQTS (V795K and E847K) or no change in the QT interval (A813K) compared to WT, while Fig. 5c shows T waves from tissues with mutations resulting in LQTS (R56Q and A797K). Note that, using our ECG delineation method, all tissue types give an upright T wave, with the exception of the V795K mutation, which gives a biphasic T wave.

Tissue vulnerability

Figure 6 shows the computed vulnerable windows for each of the tissue types, mapped out as space-time plots. The spatio-temporal size of the vulnerable window (the grey area in each panel of Fig. 6) is an index of the potential of any cellular electrophysiological abnormalities during the repolarisation phase (e.g. an ectopic focus caused by early or delayed afterdepolarisations, or by triggered activity) to initiate re-entrant propagation. As such, an increase in the size of the vulnerable window is considered pro-arrhythmic while a reduction is seen as anti-arrhythmic. On the assumption that ectopic trigger activity is equally likely to occur anywhere in the ventricular wall, this can be quantified by normalising this area with respect to the vulnerable window of the WT tissue, to give an increase/decrease in the probability of a re-entrant arrhythmia. The A795K mutation gives the largest vulnerable window (1.22 times the size of

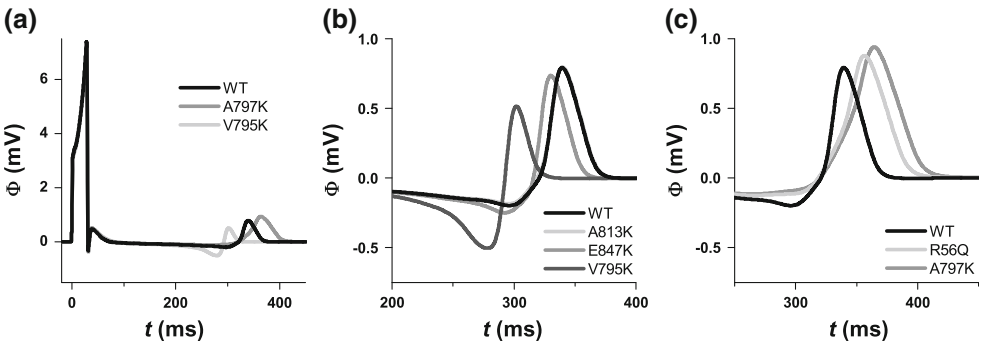

Fig. 5 **a–c** Pseudo-ECGs recorded from virtual tissues paced at a cycle length of 1 s. **a** ECGs from WT tissue and A797K and V795K mutant tissues. **b**, **c** Detailed views of the T waves from mutant tissues that result in short and long QT intervals respectively, with WT shown in both panels as a reference

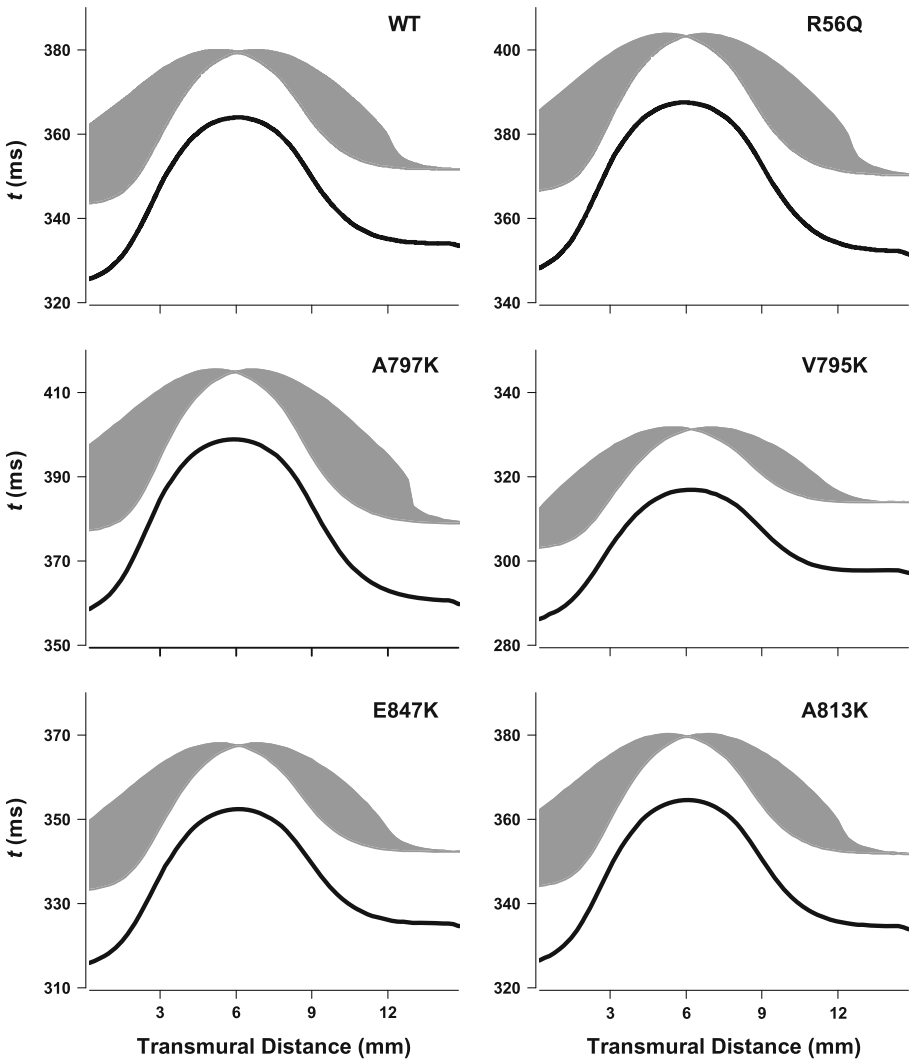

Fig. 6 Space-time plots of vulnerable windows in WT and mutant virtual tissues. The *black line* in each panel represents time of 90% repolarisation along the tissue strand. The *grey area* shows the vulnerable window, defined as the spatio-temporal region where an ectopic stimulus elicits unidirectional propagation

the WT vulnerable window), followed in descending order by R56Q (1.12), A813K (0.98), E847K (0.89) then V795K (0.64). As with APD and QT interval prolongations, the mutations that result in an increase in the vulnerable window compared to WT are those that cause a reduction in I_{Kr} maximum conductance (i.e. A795K and R56Q). All other mutations reduce the vulnerable window size.

Because the spatio-temporal distribution of the vulnerable window is determined by the repolarisation sequence across the tissue, it is reasonable to assume that vulnerable window size would be correlated to some degree with transmural dispersion of repolarisation (TDR; the time difference between the earliest and latest repolarisations): experimentally, the temporal width of the ECG T wave (Arini et al. 2008) and its time from peak to end (Antzelevitch et al. 2007b) have been proposed as measures of TDR, and changes to the QT interval and T wave morphology have been linked to arrhythmogenesis (Lawrence et al. 2005). An ECG marker could therefore provide a clinically measurable index of tissue vulnerability to arrhythmia. The relationships among TDR, vulnerability and pseudo-ECG markers are examined in Fig. 7. Cell and tissue TDR are well correlated, as would be expected, but electrotonic interactions reduce the tissue TDR. Tissue vulnerability correlates more closely with cell rather than tissue TDR. The T wave width does not correlate with vulnerability, mainly due to the biphasic T wave obtained with the V795K mutation, but both T_{peak}–T_{end} and the QT interval correlate closely with vulnerability, with the QT interval providing a slightly better correlation.

Alternans

Action potential duration alternans characterised using a dynamic restitution protocol are found in both WT and mutant virtual cells. Figure 8a shows examples of alternans recorded from an endocardial cell with the A797K mutation at a pacing cycle length of 280 ms. Figure 8b, c shows

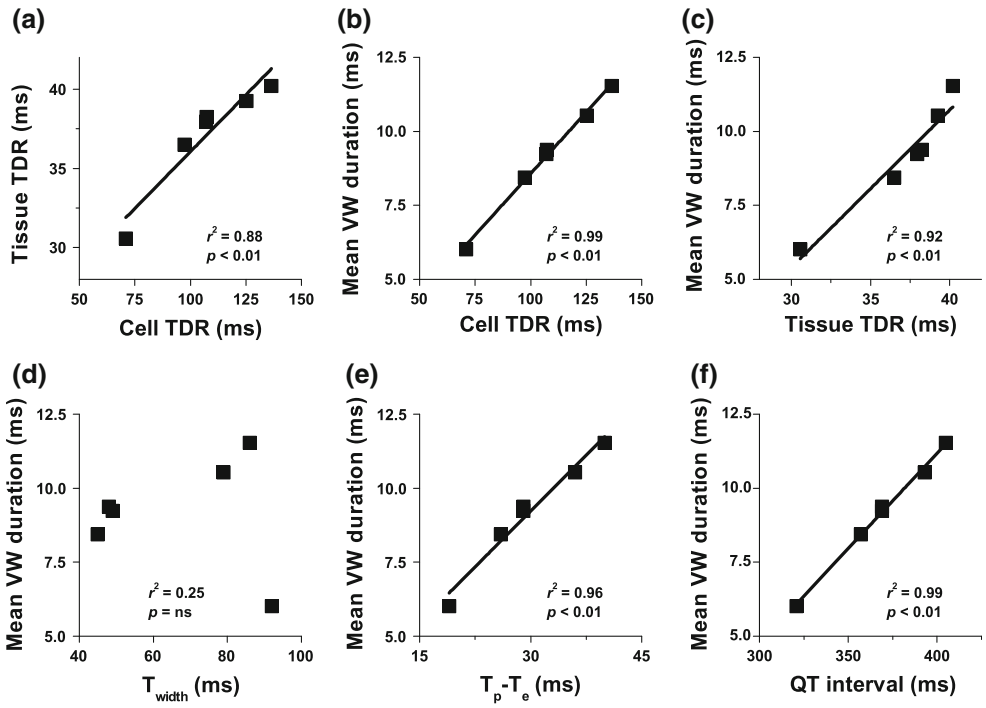

Fig. 7 Relationships among TDR, the vulnerable window (*VW*) width and various ECG intervals, from WT and mutant cells and tissues

restitution curves for WT and mutant endocardial cells. Note that the pacing cycle length at which alternans first appear follows changes seen in APD (compare with Fig. 4)—alternans first appear in WT at a cycle length of 260 ms, while with the A797K mutation they first appear at 300 ms, and with the V795K at 220 ms. All mutations increase the range of pacing cycle lengths over which alternans appear in the endocardial cells, with WT having the smallest range (25 ms) and the V795 mutation the largest (70 ms), while the temporal heterogeneity of the alternans (i.e. the maximum difference between the long and short APDs) in the endocardial cells is increased compared to WT with one mutation (A797K, from 73 ms to 91 ms) and decreased with all other mutations (R56Q reduces to 6 ms; of the de novo mutations, V795K has the largest decrease, to 41 ms). These relationships hold, at least qualitatively, in the M and epicardial cell types, with the exception of the V795K mutation, which does not cause alternans in epicardial cells and gives only a 6 ms APD difference in M cells (this has implications for emergence of discordant alternans in tissue; see below). Activation kinetics were the main influence on emergence of alternans in cells—faster activation kinetics, seen with all mutations, caused alternans to appear over an increased range of pacing cycle lengths.

The alternans observed in single cells were suppressed when the mutations were incorporated into tissues except, interestingly, with the V795K mutation. In the tissue with this mutation, the spatial and temporal heterogeneity in APD alternans resulted in the emergence of concordant or discordant alternans, depending on cycle length. Figure 9 shows examples of concordant and discordant alternans in tissue with the V795K mutation, obtained using a dynamic restitution protocol. The concordant alternans were recorded at a cycle length of 750 ms, the discordant alternans at a cycle length of 730 ms. Panel a shows example action potentials from consecutive beats, recorded from nodes located at the endocardial and epicardial ends of the strand, while panel b shows all APDs along the strand for the same two consecutive beats. For concordant alternans the entire tissue has a short APD for one beat, then a long APD for the following beat, followed again by a short APD, and so on. For discordant alternans there is a region of tissue with a long APD and a separate region with a short APD on each beat. These long and short APD regions swap locations every beat and are separated by a node with a constant APD, here located approximately 4 mm from the endocardial end of the tissue. Panel c shows repolarisation times along the strands, a functionally more relevant measure as it is these repolarisation times that determine TDR. The tissue with concordant alternans shows a small TDR (7 ms for the "odd" beat), but due to the presence of the long and short APD regions during a single beat, the tissue with discordant alternans shows a marked increase in TDR, especially when the long APD region is located epicardially (i.e. the "even beat", which has a TDR of 22 ms). As shown in Fig. 7c and in previous experimental studies (e.g. Pastore et al. 1999), increasing TDR increases the width of the vulnerable window, and so increases the probability of

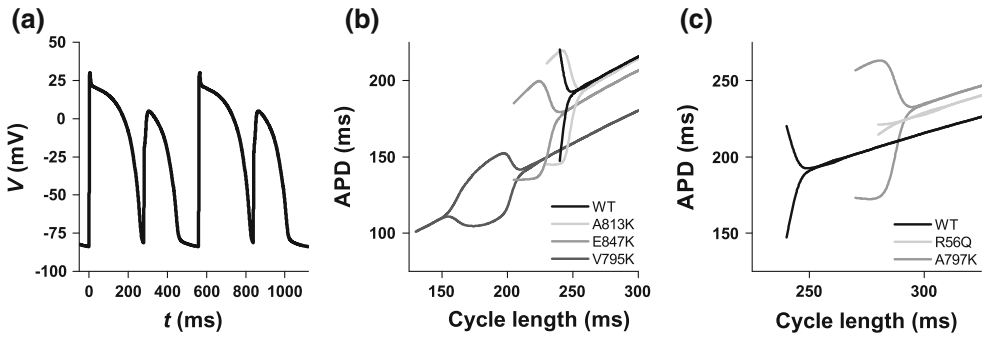

Fig. 8 **a** Example of electrical alternans in an A797K endocardial cell at a pacing cycle length of 280 ms, showing long followed by short action potentials. **b**, **c** Restitution curves obtained using a dynamic restitution protocol in endocardial cells with the short and long QT mutations respectively, with WT shown in both panels as a reference

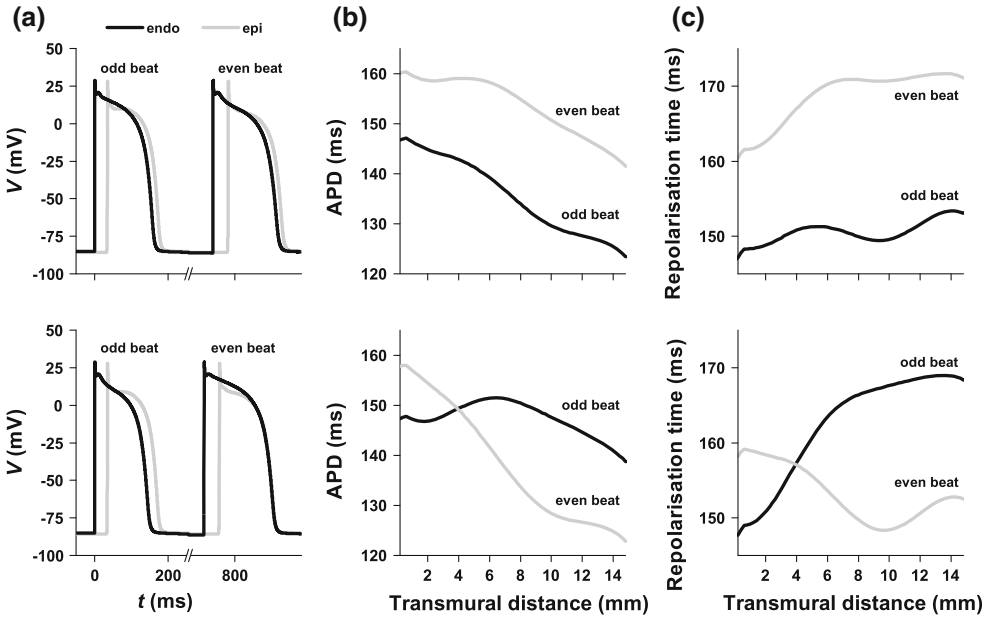

Fig. 9 Concordant (*top*) and discordant (*bottom*) alternans in virtual tissue with the V795K mutation. Pacing cycle lengths were 750 ms for the concordant alternans and 730 ms for the discordant alternans. **a** Example action potentials from subsequent beats, shown from nodes located at the endocardial (*endo*) and epicardial (*epi*) ends of the strand. Note the break in the abscissa. **b** APDs along the strand for two consecutive beats. **c** 90% repolarisation times along the strands for two consecutive beats

any arrhythmogenic triggers initiating re-entrant arrhythmias. Thus, it appears that heterogeneous emergence of alternans in single cells leads to the emergence of discordant alternans at the tissue level, and that this increases the vulnerability to arrhythmias.

Discussion

The single-cell simulation results (Fig. 4), when taken in the context of the underlying changes to I_{Kr}, are all consistent with earlier numerical studies of APD changes when I_{Kr} parameters are altered in isolation or in combinations in human (Benson et al. 2007, 2009; Peitersen et al. 2008; Fink et al. 2006; Grandi et al. 2009; Priebe and Beuckelmann 1998) and other (e.g. Benson et al. 2008; Zeng et al. 1995) ventricular cell models. Here we have shown that, in the Ten Tusscher and Panfilov model (Ten Tusscher and Panfilov 2006): (1) mutations resulting in decreased I_{Kr} maximum channel conductance result in an increased APD, regardless of any faster activation kinetics or positive shifts in the inactivation curve; (2) mutations causing a positive shift in the inactivation curve, but with no decrease in maximum channel conductance, result in a decreased APD, with the magnitude of the reduction dependent on the magnitude of the inactivation curve shift; and (3) mutations that result only in faster activation kinetics cause very little or no change in APD. Thus, from channel kinetic data we could predict that a mutation would result in SQTS unless channel conductance was reduced, when LQTS would result. In future work, we will examine the roles that I_{Kr} formulation and action potential morphology have on the emergence of LQTS and SQTS, and how sensitive any APD changes are to given I_{Kr} parameter changes in different models of human ventricular myocytes. In particular, we will compare the model used in the present study to modified versions of the same model but with different formulations for I_{Kr} (e.g. Fink et al. 2006), and to completely different human biophysical models (e.g. Grandi et al. 2009; Priebe and Beuckelmann 1998; Iyer et al. 2004) that have different (e.g. more triangular) action potential shapes.

Interestingly, with these particular mutations and this model, cell TDR correlates more closely with vulnerable window width than tissue TDR does, despite the vulnerable

window being a tissue-level phenomenon influenced by the repolarisation sequence across the ventricular wall. However, the vulnerable window is not only an index of repolarisation time and tissue TDR, it takes into account other electrophysiological phenomena that may contribute to unidirectional block, such as action potential triangulation, alteration to the refractory period, or discordant alternans that occur during the pacing sequence. This may also explain the correlation between ECG T_{peak}–T_{end} and vulnerability, and the finding that the QT interval (an index of maximum APD rather than TDR) gave the best correlation with the vulnerable window width. Here we demonstrated for the Ten Tusscher and Panfilov model (Ten Tusscher and Panfilov 2006) that cell TDR and QT interval are the best predictors of tissue vulnerability. It remains to be tested in other biophysical models of human ventricular myocytes (Fink et al. 2006; Grandi et al. 2009; Priebe and Beuckelmann 1998; Iyer et al. 2004) whether cellular TDR and the QT interval are indeed better predictors of tissue vulnerability that tissue TDR or T_{peak}–T_{end}.

The correlation of vulnerable window width and the QT interval (Fig. 7f) may initially seem strange, as SQTS can be arrhythmogenic, yet we predicted a reduced vulnerable window (i.e. less arrhythmogenic) for all mutations that cause SQTS. It should be noted, however, that the vulnerable windows measured in this study were at a pacing cycle length of 1,000 ms, and that the SQTS mutations generally result in larger cellular alternans over a greater range of cycle lengths than the LQTS mutations (Fig. 8). Furthermore, the V797K mutation was the only one to display alternans in the tissue, with concordant or discordant alternans emerging depending on pacing cycle length (Fig. 9). Thus, it is important to take into account that certain substrates for arrhythmias may only manifest under certain pacing rate conditions, and a variety of different measures (Lawrence et al. 2005) may help to define the arrhythmogenicity of a particular mutation.

The results of the current study demonstrate the effect of mutations in the hERG gene on heterogeneous tissue systems, and they therefore provide confirmation of the linkage from mutations at the genetic level, through the structural and cellular levels, to the tissue level in cardiac systems. Moreover, they provide validation of the utility of cellular electrophysiological investigations in studies of cardiac disease, by highlighting the electrophysiological differences a single mutation can cause at the channel, cell and tissue levels. This work builds on previous studies (Al-Owais et al. 2009; Benson et al. 2009) in which the effects of a variety of hERG mutants were examined. The present and these previous studies demonstrated a range of effects on cardiac activity which lead to either lengthening or, more surprisingly, shortening of the cardiac APD. However, the differences in the effects of the hERG mutations in the modelled endocardial, M and epicardial tissues highlight the limitations associated with relying solely on electrophysiological results to investigate such a complex environment as cardiac tissue (see the spatially heterogeneous emergence of alternans with the V795K mutation in section "Alternans" as an example). Certainly, the additional insight provided by the computational models used in this study will prove useful in understanding the relationship between experimental electrophysiology results and the related clinical manifestation of conditions such as LQTS and SQTS, and will provide an intriguing basis for future electrophysiological investigations, which may focus on attempting to differentiate the potentially subtle, yet possibly important, differences in the effects of mutations on different cardiac tissues. Furthermore, it appears that electrophysiology can only go so far in elucidating the manifestation of genetic changes in cardiac tissue. Indeed, the use of emerging techniques such as three-dimensional optical imaging (Walton et al. 2010)—which can give spatial as well as temporal information on the propagation of action potentials in cardiac tissues—in conjunction with existing computational models (Clayton et al. 2011) will make possible a generation of more refined three-dimensional models of cardiac activity that are informed by spatio-temporal experimental data and that may prove a useful tool in dissecting the complex regulation of cardiac activity.

Clinical implications

Mutations in hERG have been implicated in inherited LQTS type 2 and SQTS type 1, and drug-induced forms of LQTS can result from often unforeseen interactions with hERG (Kannankeril and Roden 2007). A greater understanding—from genetics through to tissue electrophysiology—will lead to clinical insight into both inherited and drug-induced forms of LQTS and SQTS. However, the QT syndromes are complex conditions, both in terms of their underlying causes and their manifestation in heterogeneous cardiac tissue. Prolongation of the cardiac action potential, for example, may be composed of multiple effects that individually lengthen or shorten the action potential (Benson et al. 2009). The use of virtual cardiac tissues, as presented in this paper, is a powerful technique that can help determine tissue level electrophysiology using subcellular kinetic measurements, and as such could be used to identify potentially pro-arrhythmic genetic mutations or drug compounds.

Limitations

Mutant hERG channels were transfected into *Xenopus* oocytes, and single-cell electrophysiology was performed

on prepared oocytes, at 21–24°C. Although this is below normal physiological temperature, we took steps to account for this temperature difference by scaling the shifts in the half inactivation voltages. Nevertheless, it is still possible that the effects of temperature-sensitive mutations in hERG may have been masked. Although the Purkinje fibre is used as a model of drug-induced LQTS in dogs (e.g. Gintant et al. 2001), and drugs that induce LQTS can induce early afterdepolarisations in rabbit Purkinje fibres (e.g. Puisieux et al. 1996), it is still unclear how hERG mutations manifest electrophysiologically in human Purkinje fibres. In a recent model of human Purkinje fibres (Stewart et al. 2009), complete block of I_{Kr} did not significantly alter automaticity or APD and did not induce afterdepolarisations. Another recent human Purkinje fibre model (Sampson et al. 2010) showed severe arrhythmogenic activity with LQTS type 3, but not with LQTS types 1 or 2. As such, and for the sake of simplicity, we do not include Purkinje fibres in our models. Limitations of using the single-cell and tissue models have been discussed in detail previously (Benson et al. 2008), and we only note here that the one-dimensional virtual tissue is a computationally efficient and simplified model of the ventricles that removes some details, such as tissue structure (Gilbert et al. 2007) and Purkinje fibres (Stewart et al. 2009; Sampson et al. 2010), that would otherwise make elucidation of tissue-level mechanisms unnecessarily complicated.

Acknowledgments This work was supported by the European Union through the BioSim Network of Excellence (contract number LSHB-CT-2004-005137). A.P.B. is supported by a Medical Research Council special training fellowship in biomedical informatics (G0701776). We acknowledge Professor Denis Wray (deceased), who initiated the research presented in this paper with support from the British Heart Foundation.

References

Akhavan A, Atanasiu R, Noguchi T, Han W, Holder N, Shrier A (2005) Identification of the cyclic-nucleotide-binding domain as a conserved determinant of ion-channel cell-surface localization. J Cell Sci 118:2803–2812

Al-Owais M, Bracey K, Wray D (2009) Role of intracellular domains in the function of the herg potassium channel. Eur Biophys J 38:569–576

Antzelevitch C, Pollevick GD, Cordeiro JM, Casis O, Sanguinetti MC, Aizawa Y, Guerchicoff A, Pfeiffer R, Oliva A, Wollnik B, Gelber P, Bonaros EP, Burashnikov E, Wu Y, Sargent JD, Schnikel S, Oberheiden R, Bhatia A, Hsu L-F, Haissaguerre M, Schimpf R, Borggrefe M, Wolpert C (2007a) Loss-of-function mutations in the cardiac calcium channel underlie a new clinical entity characterized by ST-segment elevation, short QT intervals, and sudden cardiac death. Circulation 115:442–449

Antzelevitch C, Sicouri S, Di Diego JM, Burashnikov A, Viskin S, Shimizu W, Yan GX, Kowey P, Zhang L (2007b) Does Tpeak-Tend provide an index of transmural dispersion of repolarization? Heart Rhythm 4:1114–1119

Arini PD, Bertran GC, Valverde ER, Laguna P (2008) T-wave width as an index of ventricular repolarization dispersion: evaluation in an isolated rabbit heart model. Biomed Signal Proc Cont 3:67–77

Benson AP, Halley G, Li P, Tong WC, Holden AV (2007) Virtual cell and tissue dynamics of ectopic activation of the ventricles. Chaos 17:015105

Benson AP, Aslanidi OV, Zhang H, Holden AV (2008) The canine virtual ventricular wall: a platform for dissecting pharmacological effects on propagation and arrhythmogenesis. Prog Biophys Mol Biol 96:187–208

Benson AP, Al-Owais M, Tong WC, Holden AV (2009) HERG effects on ventricular action potential duration and tissue vulnerability: a computational study. Lect Notes Comput Sci 5528:172–181

Berecki G, Zegers JG, Verkerk AO, Bhuiyan ZA, De Jonge B, Veldkemp MW, Wilders R, Van Ginneken ACG (2005) HERG channel (dys)function revealed by dynamic action potential clamp technique. Biophys J 88:56–578

Brugada R, Hong K, Dumaine R, Cordeiro J, Gaita F, Borggrefe M, Menendez TM, Brugada J, Pollevick GD, Wolpert C, Burashnikov E, Matsuo K, Sheng Wu Y, Guerchicoff A, Bianchi F, Giustetto C, Schimpf R, Brugada P, Antzelevitch C (2004) Sudden death associated with short-QT syndrome linked to mutations in HERG. Circulation 109:30–35

Chen J, Zou A, Spawski I, Keating M, Sanguinetti MC (1999) Long QT syndrome-associated mutations in the Per-Arnt-Sim (PAS) domain of HERG potassium channels accelerate channel deactivation. J Biol Chem 274:10113–10118

Clayton RH, Bernus OV, Cherry EM, Dierckx H, Fenton FH, Mirabella L, Panfilov AV, Sachse FB, Seeman G, Zhang H (2011) Models of cardiac tissue electrophysiology: progress, challenges and open questions. Prog Biophys Mol Biol 104:22–48

Cui J, Kagan A, Qin D, Mathew J, Malman TF, McDonald TV (2001) Analysis of the cyclic nucleotide binding domain of the HERG potassium channel and interactions with KCNE2. J Biol Chem 276:17244–17251

Durrer D, Van Dam RT, Freud GE, Janse MJ, Meijier FL, Arzbaecher RC (1970) Total excitation of the isolated human heart. Circulation 41:899–912

Fink M, Giles WR, Noble D (2006) Contributions of inwardly rectifying K+ currents to repolarization assessed using mathematical models of human ventricular myocytes. Philos Trans R Soc A 364:1207–1222

Finlayson K, Witchel HJ, McCulloch J, Starkey J (2004) Acquired QT interval prolongation and HERG: implications for drug discovery and development. Eur J Pharmacol 500:129–142

Fossa A, Wisialowski T, Wolfgang E, Wang E, Avery M, Raunig DL, Fermini B (2004) Differential effects of HERG blocking agents on cardiac electrical alternans in guinea pig. Eur J Pharmacol 486:209–221

Gilbert SH, Benson AP, Li P, Holden AV (2007) Regional localisation of left ventricular sheet structure: integration with current models of cardiac fibre, sheet and band structure. Eur J Cardiothorac Surg 32:231–249

Gintant GA, Limberis JT, McDermott JS, Wegner CD, Cox BF (2001) The canine Purkinje fiber: an in vitro model system for acquired long QT syndrome and drug-induced arrhythmogenesis. J Cardiovasc Pharm 37:607–618

Glukov AV, Fedorov VV, Lou Q, Ravikumar VK, Kalish PW, Schuessler RB, Moazami N, Efimiov IR (2010) Transmural dispersion of repolarisation in failing and nonfailing human ventricle. Circ Res 106:981–991

Grandi E, Pasqualini FS, Bers DM (2009) A novel computational model of the human ventricular action potential and Ca transient. J Mol Cell Cardiol 48:112–121

Hund TJ, Kucera JP, Otani NF, Rudy Y (2001) Ionic charge conservation and long-term steady state in the Luo-Rudy dynamic cell model. Biophys J 281:3324–3331

Iyer V, Mazhari R, Winslow RL (2004) A computational model of the human left-ventricular epicardial myocyte. Biophys J 87:1507–1525

Jalife J (2000) Ventricular fibrillation: mechanisms of initiation and maintenance. Annu Rev Physiol 62:25–50

Kannankeril PJ, Roden DM (2007) Drug-induced long QT and torsade de pointes: recent advances. Curr Opin Cardiol 22:39–43

Lawrence CL, Pollard CE, Hammond TG, Valentin J-P (2005) Nonclinical proarrhythmia models: predicting torsades de pointes. J Pharmacol Toxicol 52:46–59

Lehmann-Horn F, Jurkat-Rott K (1999) Voltage-gated ion channels and hereditary disease. Physiol Rev 79:1317–1372

Martínez JP, Almeida R, Olmos S, Rocha AP, Laguna P (2004) A wavelet-based ECG delineator: evaluation on standard databases. IEEE Trans Biomed Eng 51:570–581

Morita H, Wu J, Zipes DP (2000) The QT syndromes: long and short. Lancet 372:750–763

Numaguchi H, Mullins FM, Johnson JP, Johns DC, Po SS, Yang IC-H, Tomaselli GF, Balser JR (2000) Probing the interactions between inactivation gating and D-sotalol block of HERG. Circ Res 287:1012–1018

Pastore JM, Girouard SD, Laurita KR, Akar FG, Rosenbaum DS (1999) Mechanism linking T-wave alternans to the genesis of cardiac fibrillation. Circulation 99:1385–1394

Peitersen T, Grunnet M, Benson AP, Holden AV, Holstein-Rathlou N-H, Olesen S-P (2008) Computational analysis of the effects of the hERG channel opener NS1643 in a human ventricular cell model. Heart Rhythm 5:734–741

Plonsey R, Barr RC (1988) Bioelectricity: a quantitative approach. Plenum, New York

Press WH, Teukolsky SA, Vetterling WT, Flannery BP (2009) Numerical recipes: the art of scientific computing, 3rd ed. Cambridge University Press, Cambridge

Priebe L, Beuckelmann DJ (1998) Simulation study of cellular electric properties in heart failure. Circulation 82:1206–1223

Puisieux FL, Adamantidis MM, Dumotier BM, Dupuis BA (1996) Cisapride-induced prolongation of cardiac action potential and early afterdepolarizations in rabbit Purkinje fibres. Br J Pharmacol 117:1377–1379

Qu Z, Garfinkel A (1999) An advanced algorithm for solving partial differential equations in cardiac conduction. IEEE Trans Biomed Eng 46:1166–1168

Qu Z, Garfinkel A, Chen P-S, Weiss JN (2000) Mechanisms of discordant alternans and induction of reentry in simulated cardiac tissue. Circulation 102:1664–1670

Recanatini M, Cavalli A, Masetti M (2008) Modeling HERG and its interactions with drugs: recent advances in light of current potassium channel simulations. Chem Med Chem 3:523–535

Rush S, Larsen H (1978) A practical algorithm for solving dynamic membrane equations. IEEE Trans Biomed Eng 25:389–392

Sampson KJ, Iyer V, Marks AR, Kass RS (2010) A computational model of Purkinje fibre single cell electrophysiology: implications for the long QT syndrome. J Physiol 588:2643–2655

Sanguinetti MC, Jiang C, Curran ME, Keating MT (1995) A mechanistic link between an inherited and an acquired cardiac arrhythmia. Cell 81:299–307

Satler CA, Walsh EP, Vesely MR, Plummer MH, Ginsburg GS, Jacob HJ (1996) Novel missense mutation in the cyclic nucleotide-binding domain of HERG causes long QT syndrome. Am J Med Genet 65:27–35

Starmer CF, Biktashev VN, Romashko DN, Stepanov MR, Makarova ON, Krinsky VI (1993) Vulnerability in an excitable medium: analytical and numerical studies of initiating unidirectional propagation. Biophys J 65:1775–1787

Stewart P, Aslanidi OV, Noble D, Noble PJ, Boyett MR, Zhang H (2009) Mathematical models of the electrical action potential of Purkinje fibre cells. Philos Trans Roy Soc A 367:2225–2255

Ten Tusscher KHWJ, Panfilov AV (2006) Alternans and spiral breakup in a human ventricular tissue model. Am J Physiol 291:H1088–H1100

Ten Tusscher KHWJ, Noble D, Noble PJ, Panfilov AV (2004) A model for human ventricular tissue. Am J Physiol 286:H1573–H1589

Thomas D, Kiehn J, Katus HA, Karle CA (2003) Defective protein trafficking in hERG-associated hereditary long QT syndrome (LQT2): molecular mechanisms and restoration of intracellular protein processing. Cardiovasc Res 60:235–241

Tseng GN (2001) I(Kr): the hERG channel. J Mol Cell Cardiol 33:835–849

Walton RD, Benoist D, Hyatt CJ, Gilbert SH, White E, Bernus O (2010) Dual excitation wavelength epi-fluorescence imaging of transmural electrophysiological properties in intact hearts. Heart Rhythm 7:1843–1849

Weiss JN, Karma A, Shiferaw Y, Chen P-S, Garfinkel A, Qu Z (2006) From pulses to pulseless: the saga of cardiac alternans. Circ Res 98:1244–1253

Zeng J, Laurita KR, Rosenbaum DS, Rudy Y (1995) Two components of the delayed rectifier K^+ current in ventricular myocytes of the guinea pig type. Theoretical formulation and their role in repolarization. Circ Res 77:140–152